Laminar flow-induced scission kinetics of polymers in dilute solutions

E. Rognin, N. Willis-Fox, T. Zhao, T. A. Aljohani, and R. Daly

Supplementary Material

1 Viscoelastic model

The aim of this section is to compare the viscoelastic stress model used in this study to the FENE-P constitutive equation commonly used for dilute polymer solutions.[1] In the FENE-P model, the evolution equation of the normalised conformation tensor is (following the notations of the main text):

$$\frac{\mathrm{D}\boldsymbol{A}}{\mathrm{D}t} = (\nabla \boldsymbol{u})^T \cdot \boldsymbol{A} + \boldsymbol{A} \cdot \nabla \boldsymbol{u} - \frac{f(\mathrm{tr}(\boldsymbol{A}))\boldsymbol{A} - \frac{1}{3\xi^2}\boldsymbol{I}}{\tau_Z} \tag{1}$$

with f a function accounting for the finite extensibility of polymer chains, defined by:

$$f(\mathrm{tr}(\boldsymbol{A})) = \frac{1 - \frac{1}{\xi^2}}{1 - \mathrm{tr}(\boldsymbol{A})} \tag{2}$$

The polymeric stress is defined by:

$$\boldsymbol{\tau}_p = 3\xi^2 \frac{\eta_p}{\tau_Z} f(\mathrm{tr}(\boldsymbol{A}))\boldsymbol{A} \tag{3}$$

We can compare the behaviour of both models in two rheological flows: a uniaxial elongational flow (along the x-axis) of strain rate $\dot{\varepsilon}$, and a simple shear of shear rate $\dot{\gamma}$. Evolution equations are integrated with a fourth order Runge-Kutta scheme.

For the uniaxial flow, the usual quantity of interest is the extensional viscosity normalised by the zero-shear viscosity, or *Trouton ratio*, Tr, defined by:

$$\mathrm{Tr} = \frac{\boldsymbol{\tau}_{p,xx} - \boldsymbol{\tau}_{p,yy}}{\eta_p \dot{\varepsilon}} \tag{4}$$

For this comparison, the polymer extensibility is $\xi = 32$ (representative of PEO 1000k), and the parameter η_E of our model is set to $6\xi^2\eta_p$, so that both models tend towards the same extensional viscosity at high strain rates. The Trouton ratio is plotted in figure S1a as a function of normalised time, $\dot{\varepsilon}t$, for a sudden elongational flow of normalised strain rate (or Weissenberg number) $\dot{\varepsilon}\tau_z = 100$. Both models show an exponential increase towards a plateau value. Notice the very stiff increase for the FENE-P model. The steady-state Trouton ratio is also plotted in figure S1d for a range of normalised strain rates. For both models, at low strain rates the

[1] Larson, R. G. & Desai, Priyanka S. 2015 Modeling the Rheology of Polymer Melts and Solutions. *Annual Review of Fluid Mechanics* **47** (1), 47–65.

Trouton ratio tends towards the Newtonian-like value of 3, while at high strain rates it shows an increase of several orders of magnitude accounting for the contribution of long, unravelled polymer chains.

Regarding the behaviour in simple shear, the shear viscosity $\boldsymbol{\tau}_{p,xy}/\dot{\gamma}$ normalised by the zero-shear viscosity η_p, and the normalised first normal-stress coefficient, Ψ_1, defined by:

$$\Psi_1 = \frac{\boldsymbol{\tau}_{p,xx} - \boldsymbol{\tau}_{p,yy}}{\eta_p \tau_Z \dot{\gamma}^2} \tag{5}$$

are plotted in figures S1b and S1c respectively, as a function of normalised time, $\dot{\gamma} t$, for a sudden shear of intensity $\dot{\gamma}\tau_z = 100$. The FENE-P model shows an overshoot for both quantities, while for our model the overshoot is less pronounced for the shear viscosity and absent for the first normal-stress coefficient. Steady-state shear viscosity and first-normal stress coefficient are plotted in figures S1e and S1f for a range of normalised shear rates. Both models show shear-thinning, which is slightly more pronounced for our model.

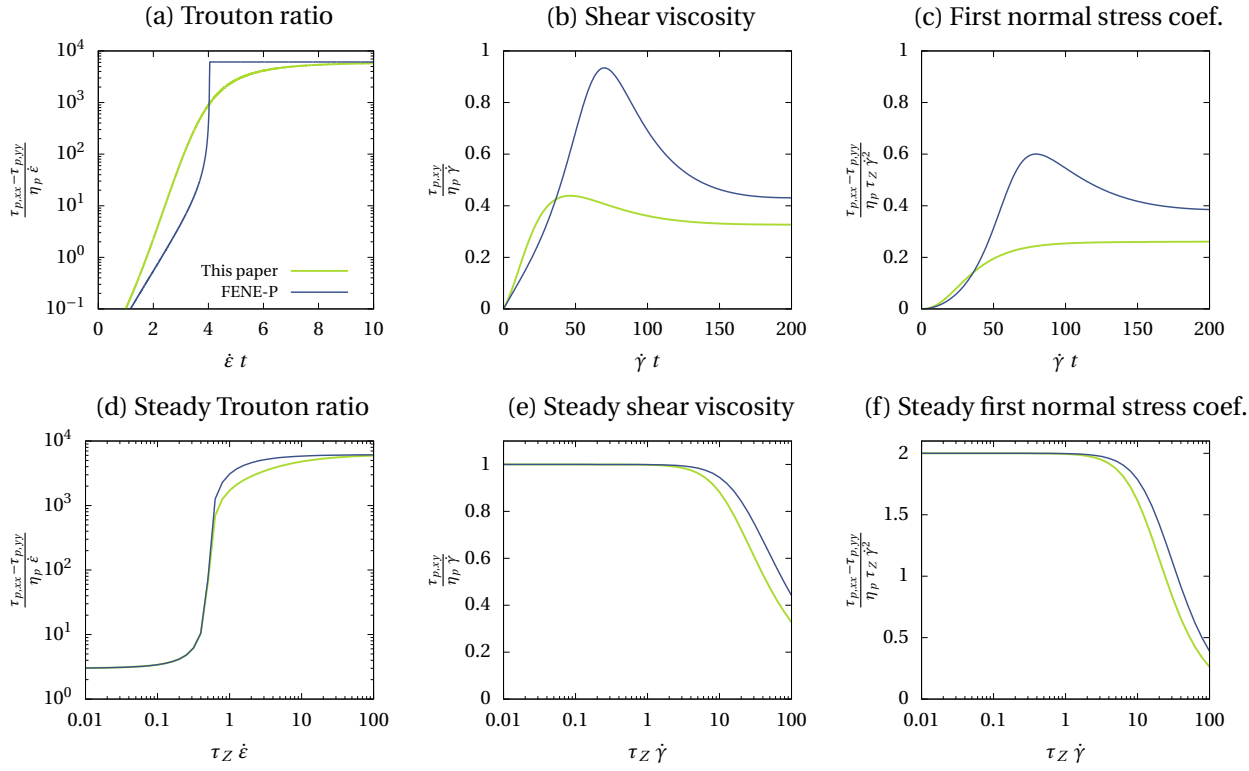

Figure S1
Comparison of the stress model used in this paper and the FENE-P model, with $\xi = 32$, $\eta_E = 6\xi^2\eta_p$, and, for transient values, $\dot{\epsilon}\tau_z = \dot{\gamma}\tau = 100$.

2 Experimental

2.1 Effect of the filters

In order to assess the effect of filters, scission experiments were done on PEO 1000k using the pinhole 50 geometry, one series with the inline filter, another series without. A third series is done by simply flowing the solution through the filter without any further constriction. The results are reported in figure S2.

- There is a non-negligible degradation at high flow rate in the filter-only configuration, although this degradation is much smaller than that caused by the pinhole.
- Degradation values are overlapping for the pinhole whether there is a filter or not: the filter is not affecting the final output.

We can explain this behaviour by two hypotheses:

- Assuming that the filter and the pinhole break random chains in the polymer population, then if for example the filter breaks 10% and the pinhole 40% at 100ml/h, the resulting degradation is 46% for both combined, which is within experimental error of the pinhole alone.
- Considering the polymer population with a certain degree of polydispersity, then assuming the filter breaks the highest molecular weights only, then the pinhole would break the remaining population subject to scission under the applied flow rate, and the surviving population would be the same regardless of the presence of a filter.

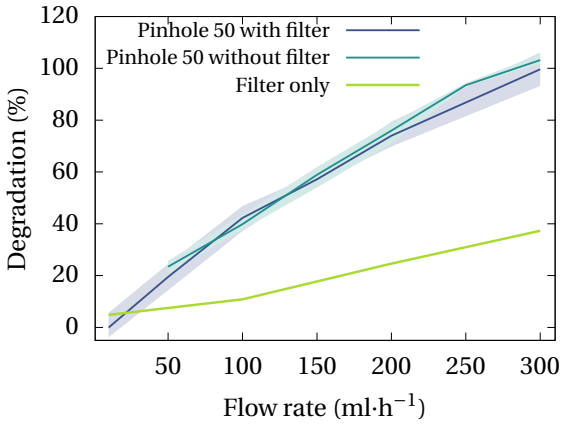

Figure S2: Degradation of PEO 1000k solutions in three cases: flow through inline filter and pinhole 50 (normal configuration), flow though pinhole 50 without filter, and flow through filter only. Experiments are run in triplicate: lines are averaged values, filled areas show extrema. Only one series is done for the filter-only configuration.

2.2 Degradation experiment results for PEO 600k and PEO 300k

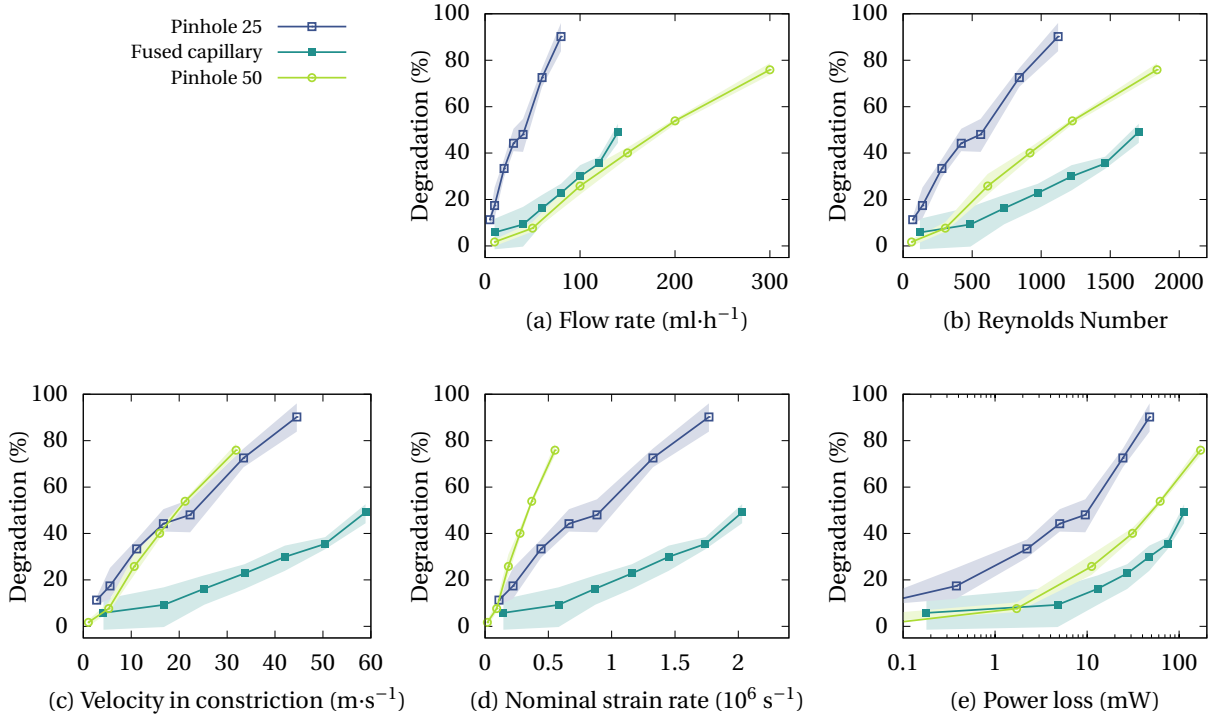

Figure S3: Degradation of PEO 600k for each constriction geometry, as a function of various characteristic parameters of the flow.

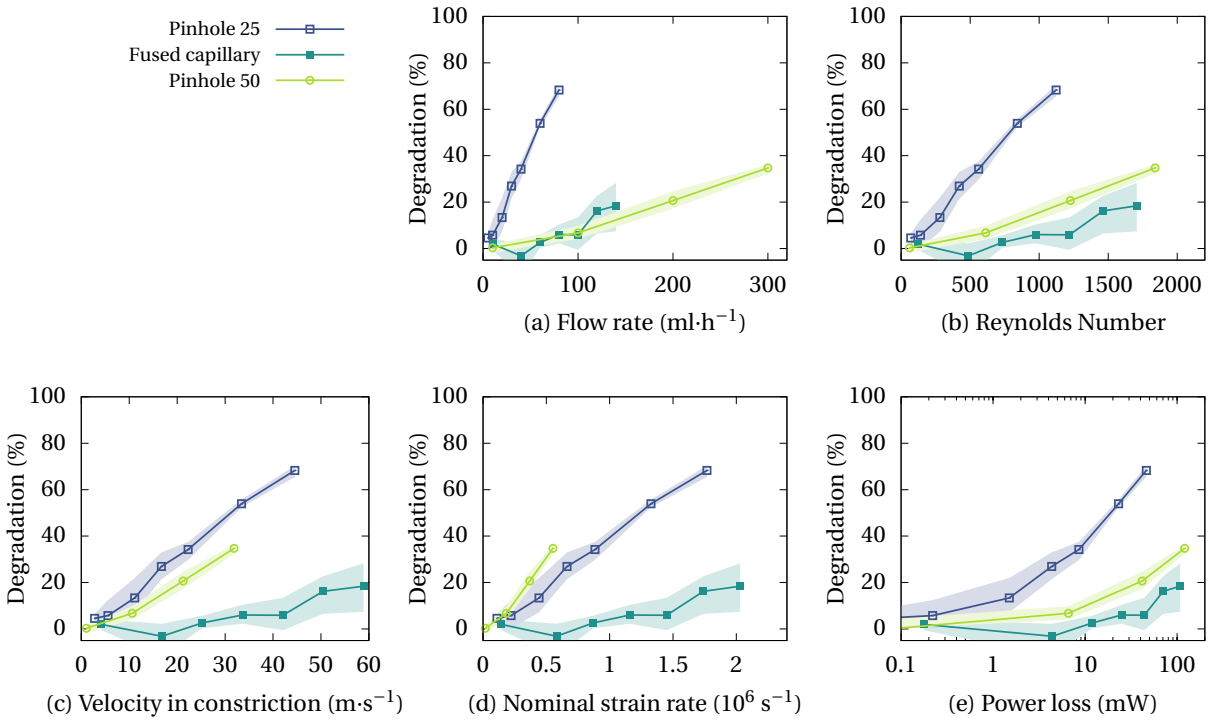

Figure S4: Degradation of PEO 300k for each constriction geometry, as a function of various characteristic parameters of the flow.

3 Nozzles characterisation

3.1 Fused glass capillary

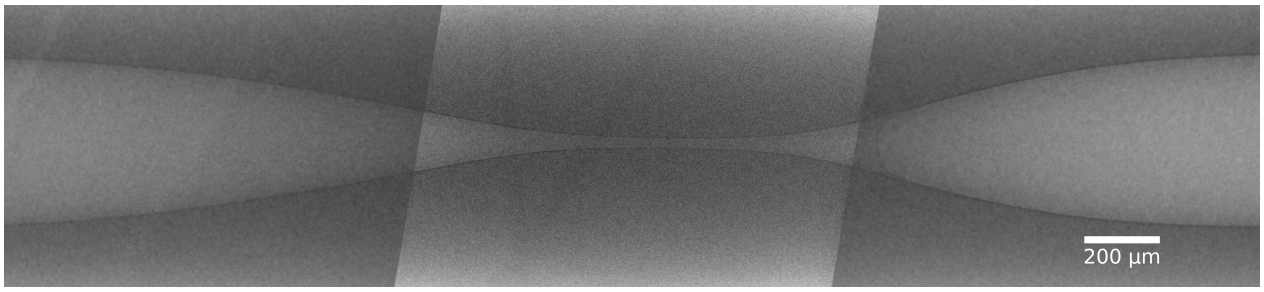

Figure S5: Fused glass capillary nozzle: X-ray absorption image (reconstructed from multiple magnifications)

(a) Mesh overview.

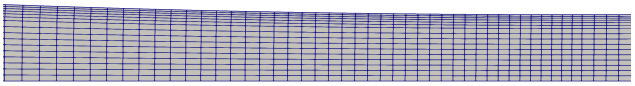

(b) Detail of the mesh in the constriction.

Figure S6: Fused glass capillary nozzle: reference axisymmetric mesh.

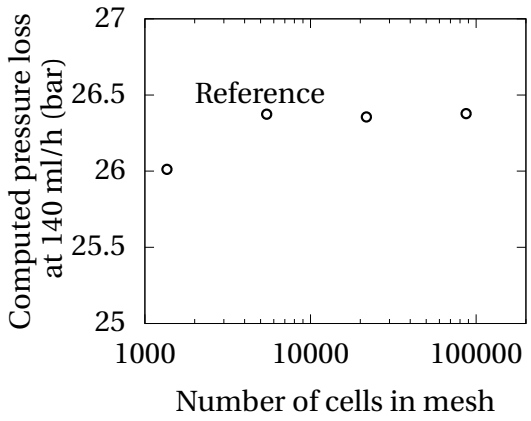

Figure S7: Fused glass capillary: mesh convergence study for the flow of water at 140 ml/h.

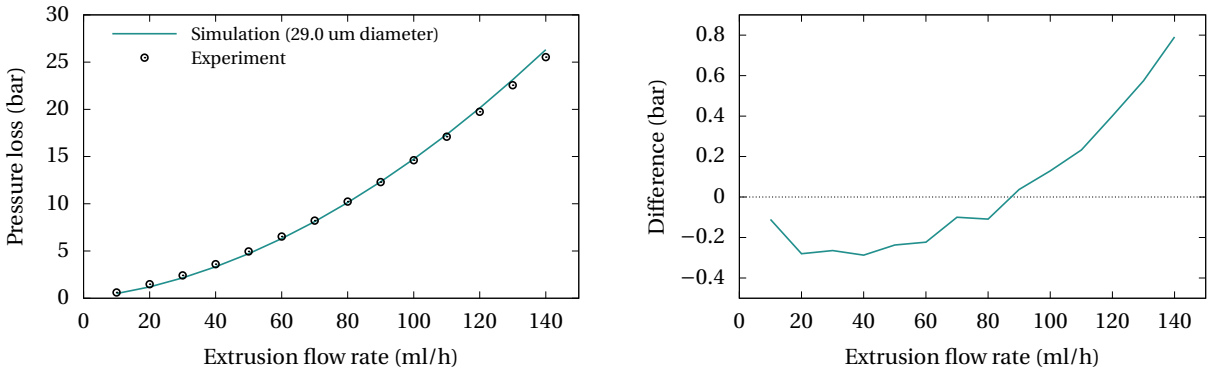

Figure S8: Fused glass capillary: contraction diameter fit with flow of water.

3.2 Pinhole 25

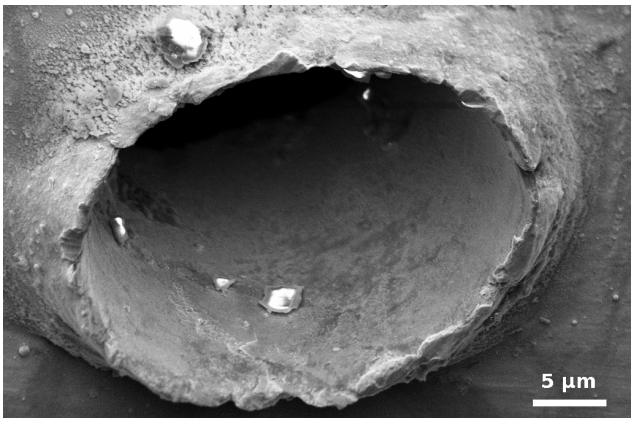

Figure S9: SEM image of the pinhole 25 (tilted view of the entrance).

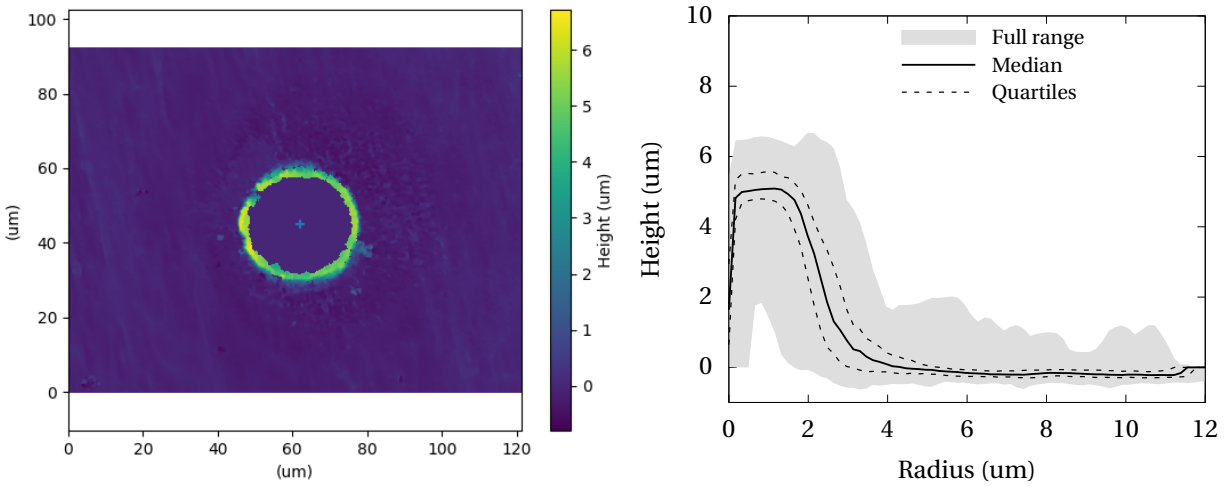

(a) Interferometry top view.

(b) Axisymmetric entrance profile (Median) extracted from interferometry.

Figure S10: Interferometry of the pinhole 25.

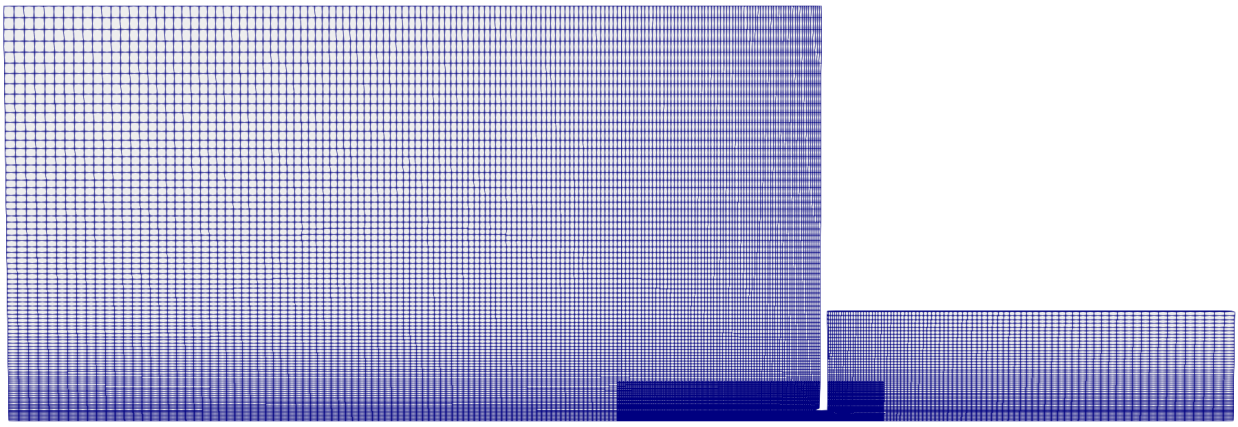

(a) Mesh overview.

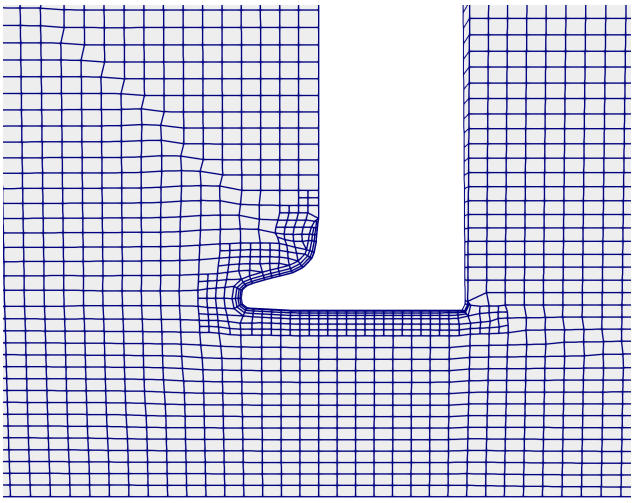

(b) Detail of the mesh in the constriction.

Figure S11: Pinhole 25: reference axisymmetric mesh.

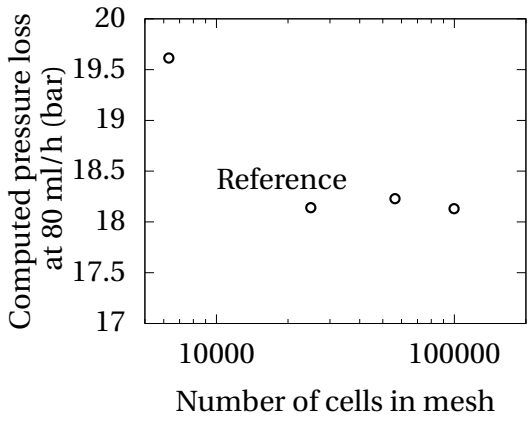

Figure S12: Pinhole 25: mesh convergence study.

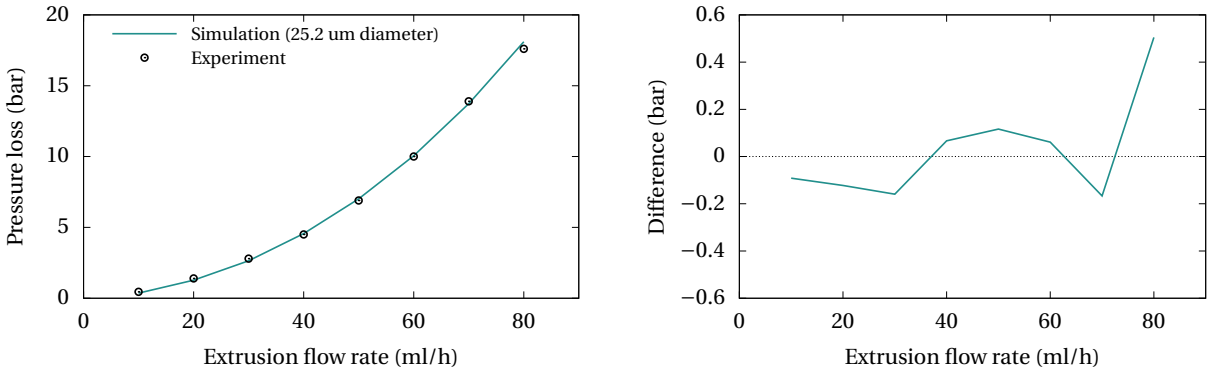

Figure S13: Pinhole 25: contraction diameter fit with flow of water.

3.3 Pinhole 50

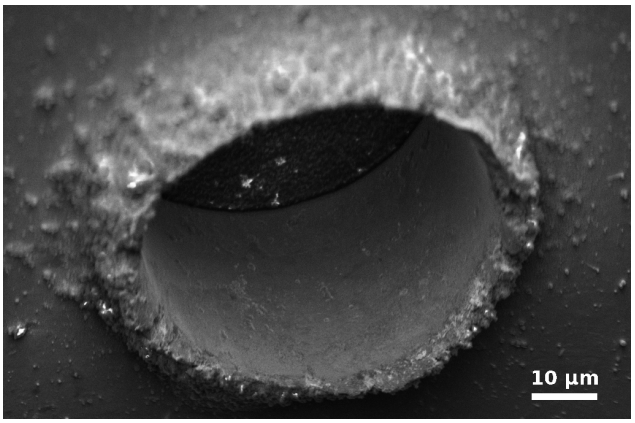

Figure S14: SEM image of the pinhole 50 µm (tilted view of the entrance).

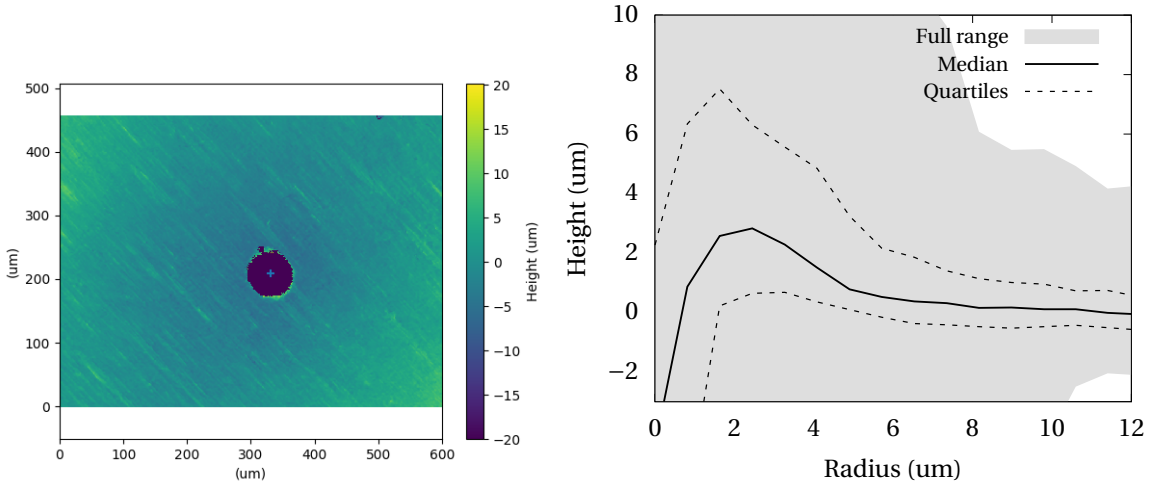

(a) Interferometry top view.

(b) Axisymmetric entrance profile (Median) extracted from interferometry.

Figure S15: Interferometry of the pinhole 50.

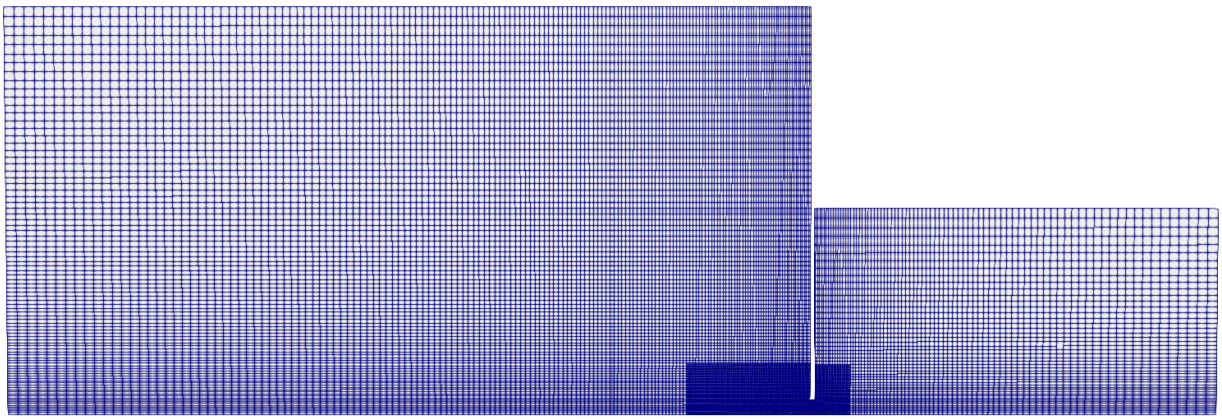

(a) Mesh overview.

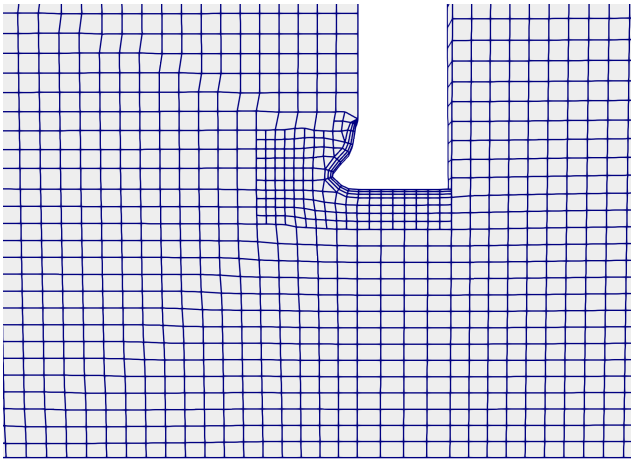

(b) Detail of the contraction

Figure S16: Pinhole 50: reference axisymmetric mesh.

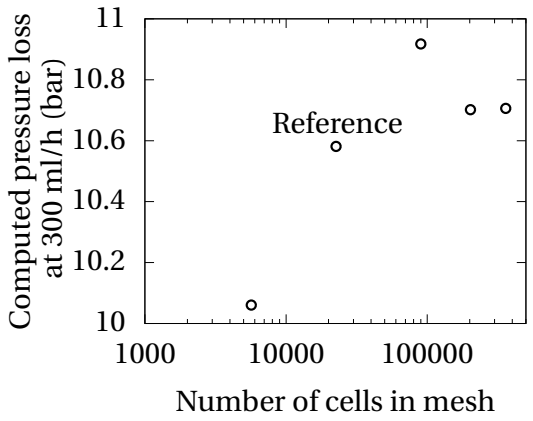

Figure S17: Pinhole 50: mesh convergence study.

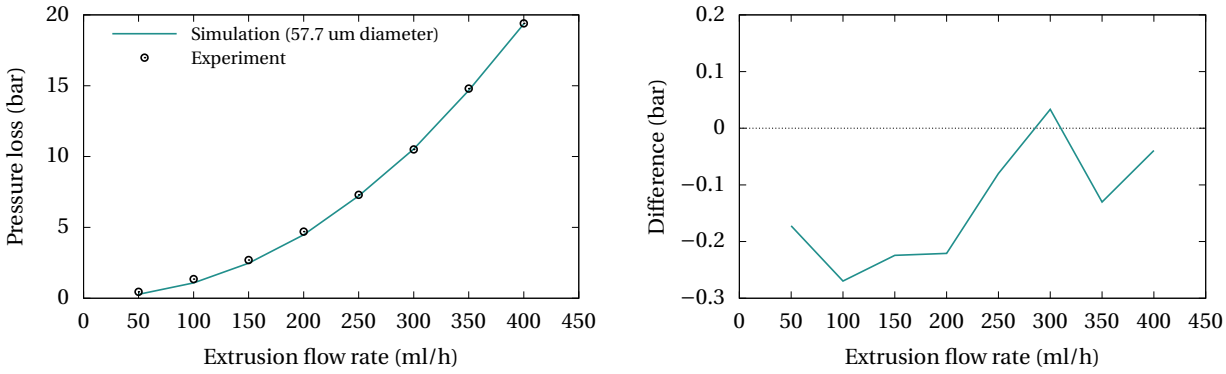

Figure S18: Pinhole 50: contraction diameter fit with the flow of water.

4 Simulation

4.1 Additional convergence tests

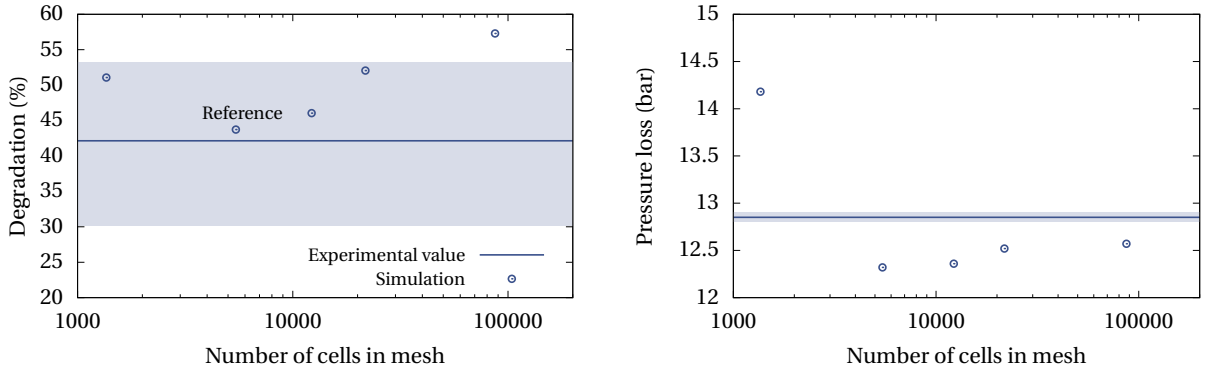

Figure S19: Mesh convergence test for the degradation of PEO 1000k in the capillary geometry at 80 ml/h. Note that a perfect fit between the reference mesh and experimental data is not expected here since the model is calibrated using multiple flow rates.

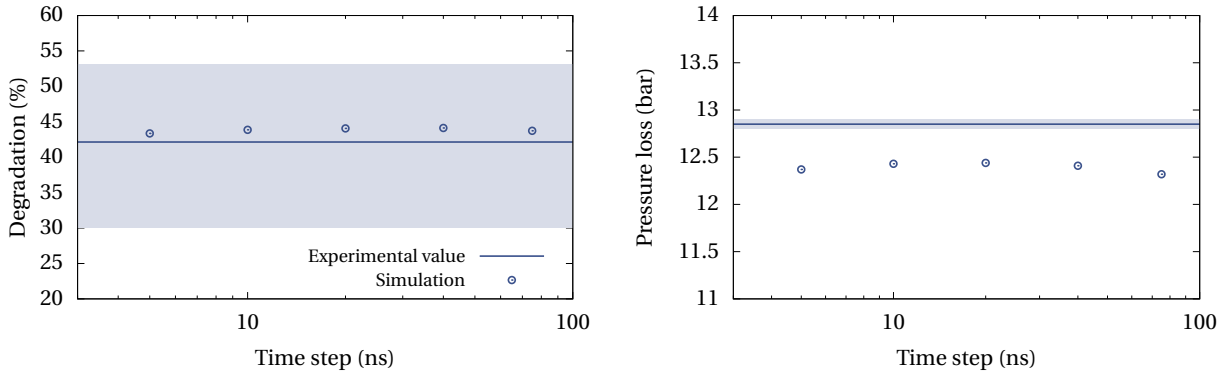

Figure S20: Time step convergence test for the degradation of PEO 1000k in the capillary geometry at 80 ml/h. The largest time step is the value used in this study (at 80 ml/h).

4.2 BSD technique

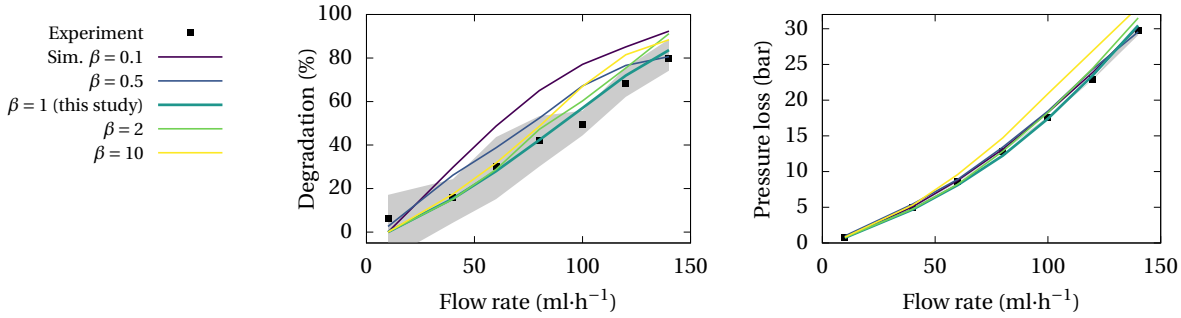

Figure S21: Effect of the BSD term on simulated degradation and pressure loss for PEO 1000k in the capillary geometry. The BSD viscosity $\eta^\star$ (eq. 4.6) is multiplied by a coefficient β. $\beta < 1$ leads to an increased chequerboard pattern producing artificially larger local strain rates. $\beta = 10$ has a significant impact on the pressure loss.